



Cite this: *Chem. Commun.*, 2024, 60, 3970

Received 7th September 2023,
Accepted 11th March 2024

DOI: 10.1039/d3cc04437h

rsc.li/chemcomm

SO₂ capture and detection with carbon microfibers (CMFs) synthesised from polyacrylonitrile†

Ana Yañez-Aulestia,^a Valeria B. López-Cervantes,^b J. Marcos Esparza-Schulz,^a Diego Solis-Ibarra,^b Ilich A. Ibarra,^{bc} Salomón Cordero-Sánchez,^{*a} Elí Sánchez-González^{id} ^{*b} and Reyna Ojeda-López^{*a}

SO₂ emissions not only affect local air quality but can also contribute to other environmental issues. Developing low-cost and robust adsorbents with high uptake and selectivity is needed to reduce SO₂ emissions. Here, we show the SO₂ adsorption–desorption capacity of carbon microfibers (CMFs) at 298 K. CMFs showed a reversible SO₂ uptake capacity (5 mmol g^{−1}), cyclability over ten adsorption cycles with fast kinetics and good selectivity towards SO₂/CO₂ at low-pressure values. Additionally, CMFs' photoluminescence response to SO₂ and CO₂ was evaluated.

Sulphur dioxide (SO₂) is a highly toxic gas that is accountable for severe respiratory illnesses, even at very low concentrations. For example, exposure to small amounts of SO₂ (as low as 1.5 ppm) for only a few minutes can cause momentary incapacity to breathe, and at higher concentrations (above 100 ppm) can cause death.¹

Different strategies to remove SO₂ (flue gas desulphurisation processes FGD) have been typically used with acceptable results. These include limestone scrubbers (producing calcium sulphite)² and even SO₂ fixation (disulfitomercurate).³ However, these procedures exhibited drawbacks associated with large amounts of wastewater, high toxicity, corrosion of pipelines, and high recuperation fees. Other SO₂ capture alternatives, such as silicas, zeolites, metal oxides, and activated

carbons, have exhibited low SO₂ efficiency.^{4,5} Although metal-organic frameworks (MOFs) have demonstrated promising SO₂ capture results, for example, MOF-177 and MIL-101(Cr) showing high SO₂ capture values, the crystal structure of these materials collapsed after being in contact with SO₂.⁶

Most of the current research on SO₂ has been narrowly focused on capturing this corrosive gas. However, the SO₂ capture is not the only relevant; SO₂ detection is as suitable as the capture and conversion of SO₂.⁷ Efficient materials for SO₂ detection are required to comply with the following characteristics: (i) high chemical stability towards SO₂ under more realistic conditions (60% of relative humidity), (ii) non-dependency on relatively high surface areas, and (iii) high processability.⁶ In addition to remarkable chemical and structural stability, such “detector materials” are characterised for showing high SO₂ uptake at low pressure, providing feasible applicability in SO₂ detection devices.⁸ Cooper *et al.* demonstrated outstanding SO₂ capture in porous organic cages (POCs) at low pressure.^{9,10} Therefore, new porous platforms have appeared as exciting alternatives to capture and detect corrosive and explosive gases. For example, Hiraoka and co-workers reported a functionalised organic nanotube with optimal selective fluorescence properties to detect liquefied petroleum gas.¹¹

Carbon materials have been explored for SO₂ capture. Yi *et al.*, tested coconut shell-based activated carbon (SAC) and coal-based activated carbon (CAC), where SAC was the best adsorbent for SO₂.¹² Muñiz *et al.* performed thermal and chemical treatments to enhance the SO₂ uptake on activated carbon fibres, and they concluded that the superficial functionalities with a basic character seem to be the most important characteristic concerning SO₂ capture.¹³ Wang *et al.*, developed a series of N-doped coal-based porous carbons (NCPs) by calcining a mixture of anthracite, MgO, KOH and carbamide at 1073 K; their results showed that the balance between nitrogen doping content and specific surface area (microporosity) improved the number of active adsorption sites of SO₂.¹⁴ In this context, the carbon microfibers (CMFs) obtained

^a Laboratorio de Físicoquímica de Superficies, Departamento de Química, Universidad Autónoma Metropolitana-Iztapalapa (UAM-I), Mexico City, CDMX 09310, Mexico. E-mail: scs@xanum.uam.mx, rol@xanum.uam.mx

^b Laboratorio de Físicoquímica y Reactividad de Superficies (LaFREs), Instituto de Investigaciones en Materiales, Universidad Nacional Autónoma de México, Circuito Exterior s/n, CU, Del Coyoacán, 04510, Ciudad de México, Mexico. E-mail: elisg@materiales.unam.mx

^c On sabbatical as “Catedra Dr Douglas Hugh Everett” at Departamento de Química, Universidad Autónoma Metropolitana-Iztapalapa, San Rafael Atlixco 186, Col. Leyes de Reforma 1ra Sección, Iztapalapa, C.P. 09310, Ciudad de México, Mexico

† Electronic supplementary information (ESI) available: CMFs synthesis, characterisation details, and additional photoluminescence experiments. See DOI: <https://doi.org/10.1039/d3cc04437h>



by calcination of polyacrylonitrile microfibers (PANMFs)¹⁵ present an opportunity for SO₂ detection due to the following aspects: (i) chemical composition based on nitrogen and oxygen functional groups resulting from the polymer precursor (PAN), (ii) high microporosity controllable depending on calcination temperature, (iii) good thermal stability, and (iv) reversible gas adsorption (e.g., CO₂ or CH₄). Concerning nitrogen functional groups, there have been identified four groups in the CMFs: N-6 (pyridine-N), N-5 (pyrrolic-N), N-X (pyridine-N-oxide) and N-Q (quaternary-N or graphitic-N).¹⁵ Some of these groups have improved the performance of CMFs in oxygen reduction reactions (ORR) in fuel cells¹⁶ and their gas adsorption properties (CO₂ and CH₄).¹⁵

Textural, chemical, and structural characterisation of the CMFs have been reported previously (Fig. S1, ESI†).¹⁷ CMFs were obtained by calcination of PANMFs at 1173 K; this material has a specific surface area of 731 m² g⁻¹, a total pore volume of 0.348 cm³ g⁻¹, and a microporosity above 70%. An average pore size of 0.78 nm was calculated from the N₂ adsorption isotherm at 77 K, and 0.5 nm was estimated using the CO₂ adsorption isotherm at 273 K.¹⁷ The CMFs average chemical composition is C: 89%, N: 6%, and O: 5%. It is important to mention that the fibrous structure of PANMFs is preserved after calcination with fibre diameters between 200 and 400 nm.

Since CMFs contain several nitrogen sites, which can be potential SO₂-adsorption sites, we measured the SO₂ adsorption

at 298, 303 and 308 K (Fig. 1a). SO₂ isotherms showed a type-I profile based on IUPAC¹⁸ with a small hysteresis. CMFs showed a maximum uptake of 5.2, 4.9 and 4.6 mmol g⁻¹ at 1 bar for 298, 303 and 308 K, respectively. This value is higher than several reported in the literature compared to other carbonaceous or inorganic materials in the function of superficial area BET (Fig. S4, ESI†). The three SO₂ adsorption isotherms were used to calculate the isosteric enthalpy of adsorption, obtaining values around -30 kJ mol⁻¹ (see Fig. S3, ESI†), consistent with a physisorption process and mild regeneration conditions.

Then, cyclability tests were carried out to evaluate the reusability of the material at the conditions where the highest SO₂ capture was obtained. Ten SO₂ adsorption-desorption cycles were performed at 298 K until 1 bar. The amount of SO₂ captured in each cycle is stable, around 5 mmol g⁻¹ (Fig. 1b). Between each cycle, a vacuum activation process was enough to desorb almost all the SO₂ adsorbed, leading to the slight increase in the baseline and thus, the maximum SO₂ uptake in each cycle.

FTIR-ATR and SEM measurements were performed to characterise the CMFs in the SO₂ capture process (Fig. 2). In the three different stages during the SO₂ uptake (before and after the first adsorption cycle and after ten desorption cycles indicated by pink, yellow and purple colours, respectively, in Fig. 1 and 2), the IR-ATR spectra showed the presence of ester groups between 2250 to 2000 cm⁻¹, and coupling C-N stretching and N-H deformation modes of C-N-H groups (amide)



Fig. 1 (a) SO₂ adsorption-desorption isotherms at 298, 303, and 308 K, (b) ten SO₂ adsorption-desorption cycles on CMFs.



Fig. 2 (a) IR-ATR spectra at different stages according to the points marked in Fig. 1b, pristine sample (pink), after SO₂ uptake (yellow), and after 10 desorption cycles (violet). SEM micrographs with their EDX results on (b) pristine sample, (c) after 10 desorption cycles, (d) after SO₂ uptake, and (e) the EDX mapping results of the rectangular area inside panel (d).



around 1522 cm^{-1} . For the SO_2 -saturated CMFs sample, a characteristic band in 1050 cm^{-1} was identified, indicating the S=O group was present (Fig. 2a).^{19,20} These results are in good agreement with the SEM micrographs and EDX analyses. Carbon microfibres morphology only changes when the SO_2 capture process occurs; the surface showed small globularities protruding from the fibre channels, and the EDX results showed sulphur presence of around 7 wt% and an increment of the oxygen percentage as well (Fig. 2d). The EDX mapping displayed a homogeneous distribution of C, N, O and S on the surface in the area shown inside the $5\text{ }\mu\text{m}$ scale micrograph in Fig. 2d. The sample showed the same morphology and composition before starting the cycles (Fig. 2b), with the sample pristine and after the last desorption cycle (Fig. 2c). These results indicate that the CMFs are stable against SO_2 for ten adsorption-desorption cycles.

Considering that SO_2 is often found as a minor component of flue gas mixtures (diluted in CO_2 and/or N_2), the separation selectivity is a crucial factor to consider. The SO_2/CO_2 separation selectivity was determined employing the ideal adsorbed solution theory (IAST) using two monocomponent isotherms of SO_2 and CO_2 at 298 K (Fig. 3a, details on ESI†). The CMFs exhibited good selectivity values for the binary mixtures SO_2/CO_2 in the low-pressure domain, 122, 118 and 110 for

1%, 5% and 10% of SO_2 at 0.05 bar, respectively (Fig. 3b). The IAST selectivity result is comparable with similar superficial area BET adsorbents such as zeolite Y ($180,930\text{ m}^2\text{ g}^{-1}$),²¹ Mg-gallate ($321,576\text{ m}^2\text{ g}^{-1}$),²² Co-gallate ($143,494\text{ m}^2\text{ g}^{-1}$),²² DMOF-TM ($169,900\text{ m}^2\text{ g}^{-1}$),²³ MIL-160 ($128,1170\text{ m}^2\text{ g}^{-1}$),²⁴ Cu-ATC ($114,600\text{ m}^2\text{ g}^{-1}$),²⁵ NbOFFIVE-Cu-TPA ($78,1179\text{ m}^2\text{ g}^{-1}$).²⁶ Granted, the SO_2 uptake of CMFs falls short in front of benchmark materials. However, these results invite us to explore another application of the CMFs, SO_2 detection, where the reversible adsorption and selectivity are relevant.

Photoluminescence experiments were carried out on the CMFs using a $\lambda_{\text{ex}} = 370\text{ nm}$ after exposure to an SO_2 -saturated atmosphere (details on ESI†). The PL intensity increased by about 50% after the SO_2 exposure, compared to the activated sample (Fig. 4a). This switch-on emission decreased over time: after 15 min of exposure, the emission returned to the value of the reference sample. However, when the sample is not activated and has been left in contact with the environment, the signal increases, indicating that it detects other molecules, such as H_2O or CO_2 . To evaluate this hypothesis, PL measurements were performed by saturating the CMFs with CO_2 and H_2O separately (Fig. S6, ESI†). The results showed a positive response for carbon dioxide but not for water. The presence of specific functional groups on carbon materials as the nitrogen-



Fig. 3 (a) Comparison of the SO_2 and CO_2 adsorption isotherms at 298 K on CMFs. (b) IAST selectivity of SO_2/CO_2 on CMFs for different concentrations of the binary mixture.

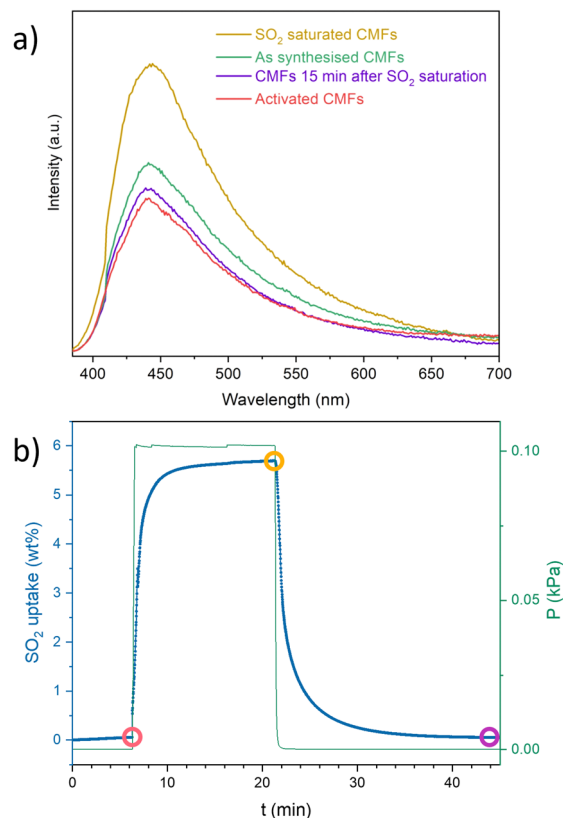


Fig. 4 (a) Photoluminescence CMFs spectra ($\lambda_{\text{ex}} = 370\text{ nm}$) of as synthesised, activated, SO_2 saturated and after the exposure to SO_2 samples. (b) Profile of adsorption-desorption kinetics of SO_2 on CMFs (gravimetric experiment with controlled SO_2 atmosphere).



bearing active sites in the CMFs (in the form of NH_2 , for example, where nitrogen acts as an electron donor) may enhance the interaction with SO_2 and the resulting photoluminescent response. The interaction between these gases with free electron pairs favours light absorption and subsequent emission for detection.²⁷ For the SO_2 interaction, the observed reversibility agrees with the observed adsorption-desorption kinetics of SO_2 obtained by gravimetric experiments (Fig. 4b). However, even though a similar PL intensity was observed for CO_2 exposed sample compared to SO_2 , the PL emission of the CO_2 exposed sample remained after several hours, indicating a slow desorption of this gas molecule (Fig. S7, ESI†).

In summary, SO_2 adsorption-desorption capacity at room temperature and 1 bar of CMFs was around 5 g mol^{-1} . It maintained good chemical and morphological stability during 10 adsorption-desorption cycles of SO_2 and a good SO_2/CO_2 selectivity, achieving a reasonable degree of reuse. When evaluating the photoluminescence of the material, it was determined that it can detect SO_2 and CO_2 but not H_2O and that SO_2 desorption is faster than CO_2 . CMFs may be functionalised to improve their textural properties, SO_2 uptake and selectivity overall.

I. A. I. thanks PAPIIT UNAM (IN201123), México, for financial support, U. Winnberg (Euro Health) for scientific discussions and G. Ibarra-Winnberg for scientific encouragement. R. O.-L. thanks are also given to the project “Medios porosos y superficies: preparación y caracterización” (UAM-I, DCBI).

Conflicts of interest

There are no conflicts to declare.

Notes and references

- 1 J. Schwartz and D. W. Dockery, *Am. Rev. Respir. Dis.*, 1992, **145**, 600–604.
- 2 F. J. Gutiérrez Ortiz, F. Vidal, P. Ollero, L. Salvador, V. Cortés and A. Giménez, *Ind. Eng. Chem. Res.*, 2006, **45**, 1466–1477.
- 3 P. W. West and G. C. Gaeke, *Anal. Chem.*, 1956, **28**, 1816–1819.
- 4 M. A. Hanif, N. Ibrahim and A. Abdul Jalil, *Environ. Sci. Pollut. Res.*, 2020, **27**, 27515–27540.
- 5 R. K. Srivastava, *Controlling SO_2 Emissions – A Review of Technologies*, DIANE Publishing, Washington, D. C., 2000.
- 6 E. Martínez-Ahumada, M. L. Díaz-Ramírez, M. de, J. Velásquez-Hernández, V. Jancik and I. A. Ibarra, *Chem. Sci.*, 2021, **12**, 6772–6799.
- 7 S. J. Rowland and J. A. F. Rook, *Int. J. Dairy Technol.*, 1961, **14**, 112–114.
- 8 V. Chernikova, O. Yassine, O. Shekhah, M. Eddaoudi and K. N. Salama, *J. Mater. Chem. A*, 2018, **6**, 5550–5554.
- 9 E. Martínez-Ahumada, D. He, V. Berryman, A. López-Olvera, M. Hernandez, V. Jancik, V. Martis, M. A. Vera, E. Lima, D. J. Parker, A. I. Cooper, I. A. Ibarra and M. Liu, *Angew. Chem., Int. Ed.*, 2021, **60**, 17556–17563.
- 10 N. K. Gupta, A. López-Olvera, E. González-Zamora, E. Martínez-Ahumada and I. A. Ibarra, *ChemPlusChem*, 2022, **87**, e202200006.
- 11 Y.-Y. Zhan, J. Liao, M. Kajita, T. Kojima, S. Takahashi, T. Takaya, K. Iwata and S. Hiraoka, *Commun. Chem.*, 2019, **2**, 107.
- 12 H. Yi, Z. Wang, H. Liu, X. Tang, D. Ma, S. Zhao, B. Zhang, F. Gao and Y. Zuo, *J. Chem. Eng. Data*, 2014, **59**, 1556–1563.
- 13 J. Muñoz, J. E. Herrero and A. B. Fuertes, *Appl. Catal., B*, 1998, **18**, 171–179.
- 14 Q. Wang, L. Han, Y. Wang, Z. He, Q. Meng, S. Wang, P. Xiao and X. Jia, *RSC Adv.*, 2022, **12**, 20640–20648.
- 15 R. Ojeda-López, J. M. Esparza-Schulz, I. J. Pérez-Hermosillo, A. Hernández-Gordillo and A. Domínguez-Ortiz, *Fibers*, 2019, **7**, 81.
- 16 R. Ojeda-López, G. Ramos-Sánchez, J. M. Esparza-Schulz, L. Lartundo and A. Domínguez-Ortiz, *Int. J. Hydrogen Energy*, 2017, **42**, 30339–30348.
- 17 R. Ojeda-López, E. Vilarrasa-García, D. C. S. Azevedo, C. Felipe, J. A. Cecilia and E. Rodríguez-Castellón, *Fuel*, 2022, **324**, 124242.
- 18 M. Thommes, K. Kaneko, A. V. Neimark, J. P. Olivier, F. Rodríguez-Reinoso, J. Rouquerol and K. S. W. Sing, *Pure Appl. Chem.*, 2015, **87**, 1051–1069.
- 19 P. Larkin, *Infrared and Raman Spectroscopy*, Elsevier, 2011.
- 20 M. R. Derrick, D. Stulik and J. M. Landry, *Infrared Spectroscopy in Conservation Science*, Getty Conservation Institute, 2000.
- 21 P. Brandt, A. Nuhnen, S. Öztürk, G. Kurt, J. Liang and C. Janiak, *Adv. Sustainable Syst.*, 2021, **5**, 2000285.
- 22 F. Chen, D. Lai, L. Guo, J. Wang, P. Zhang, K. Wu, Z. Zhang, Q. Yang, Y. Yang, B. Chen, Q. Ren and Z. Bao, *J. Am. Chem. Soc.*, 2021, **143**, 9040–9047.
- 23 S. Xing, J. Liang, P. Brandt, F. Schäfer, A. Nuhnen, T. Heinen, I. Boldog, J. Möllmer, M. Lange, O. Weingart and C. Janiak, *Angew. Chem., Int. Ed.*, 2021, **60**, 17998–18005.
- 24 P. Brandt, A. Nuhnen, M. Lange, J. Möllmer, O. Weingart and C. Janiak, *ACS Appl. Mater. Interfaces*, 2019, **11**, 17350–17358.
- 25 Z. Zhu, K. Wu, X. Liu, P. Zhang, S. Chen, J. Chen, Q. Deng, Z. Zeng, S. Deng and J. Wang, *AIChE J.*, 2022, **68**, e17811.
- 26 W. Xu, L. Li, M. Guo, F. Zhang, P. Dai, X. Gu, D. Liu, T. Liu, K. Zhang, T. Xing, M. Wang, Z. Li and M. Wu, *Angew. Chem., Int. Ed.*, 2023, **62**, e202312029.
- 27 X. Zhang, B. Yang, X. Wang and C. Luo, *Sensors*, 2012, **12**, 9375–9385.

